iJRASET
International Journal For Research in Applied Science and Engineering Technology

INTERNATIONAL JOURNAL FOR RESEARCH

IN APPLIED SCIENCE & ENGINEERING TECHNOLOGY

Volume: 14 **Issue:** II **Month of publication:** February 2026

DOI: https://doi.org/10.22214/ijraset.2026.77509

www.ijraset.com

Call: 08813907089 | E-mail ID: ijraset@gmail.com

International Journal for Research in Applied Science & Engineering Technology (IJRASET)
ISSN: 2321-9653; IC Value: 45.98; SJ Impact Factor: 7.538
Volume 14 Issue II Feb 2026- Available at www.ijraset.com

Green-Mediated Co-Precipitation Synthesis of $CoWO_4$/gCN Nanocomposites for Rose Bengal Photocatalytic Degradation

Priyanka[1], Dr. Heena Dahiya[2]
[1]*Research Scholar,* [2]*Assistant Professor, Department of Chemistry, Baba Mastnath University, Rohtak, Haryana (INDIA)*

Abstract: ***In the present study, high-performance cobalt tungstate/graphitic carbon nitride ($CoWO_4$/gCN) binary nanocomposites were successfully synthesized through a low-cost, green co-precipitation route assisted by* Phoenix dactylifera *L. fruit extract. The plant extract acted as an eco-friendly reducing and fuel agent, eliminating the need for toxic chemicals while promoting controlled nucleation, particle growth and effective interfacial coupling between $CoWO_4$ and gCN. Structural and compositional analyses using XRD, FE-SEM, TEM, XPS, EDAX and elemental mapping confirmed the formation of phase-pure monoclinic $CoWO_4$ uniformly anchored onto gCN sheets. UV–Vis diffuse reflectance spectroscopy revealed enhanced visible-light absorption with a narrowed band-gap energy in the range of 2.3–2.55 eV, attributed to heterojunction formation and improved charge separation. Photocatalytic evaluation using Rose Bengal dye under visible-light irradiation demonstrated outstanding activity, achieving ~81.01 % degradation within 75 min and maintaining ~78 % efficiency after three consecutive cycles, indicating excellent stability and reusability. Compared with conventional $CoWO_4$-based photocatalysts, the present system exhibits superior efficiency through sustainable synthesis and effective charge-transfer pathways, underscoring its potential for visible-light-driven wastewater remediation.***

Keywords: Cobalt tungstate; g-C_3N_4; green synthesis; date palm extract; binary nanocomposite; photocatalysis; Rose Bengal degradation; visible light.

Highlights

- Microwave-assisted green synthesis of $CoWO_4$ and $CoWO_4$/gCN nanocomposites using date palm extract.
- Facilitates heterojunction formation without the use of conventional chemical reagents.
- XRD, SEM, XPS, EDAX and elemental mapping confirm structure and composition, surface morphology/shape.
- $CoWO_4$/g-C_3N_4 shows enhanced visible-light-driven Rose Bengal degradation (%) with time.
- Binary nanocomposite exhibits high stability and reusability over multiple cycles.

I. INTRODUCTION

Nanotechnology has become a key area of modern materials research due to the distinctive physicochemical properties exhibited by materials at the nanoscale, where particle size, morphology and interfacial interactions strongly influence functional behavior [1,2]. Within this field, nanocomposites have attracted particular interest because the combination of multiple components often produces synergistic effects, such as improved charge transport [3,4], enhanced surface activity and superior optical properties [5,6]. These advantages make nanocomposites highly promising for environmental and energy-related applications [7-11]. Among various semiconductor materials, metal tungstates (AWO_4) have been widely investigated owing to their chemical stability, suitable electronic structures and multifunctional characteristics [12]. Cobalt tungstate ($CoWO_4$), a p-type semiconductor with a wolframite structure, has demonstrated potential in photocatalysis, electrochemical devices, pigments and dielectric materials [13,14]. However, the photocatalytic efficiency of pristine $CoWO_4$ is often limited by rapid recombination of photogenerated electron–hole pairs and inadequate visible-light absorption, which restricts its effectiveness in environmental remediation. To address these limitations, heterostructured nanocomposites [15-18] have emerged as an efficient strategy. Graphitic carbon nitride (gCN), commonly represented by its chemical formula g-C_3N_4, is a metal-free polymeric semiconductor known for its visible-light activity, chemical stability, low cost, and environmental compatibility.

Nevertheless, pristine gCN suffers from low surface area and inefficient charge separation. Coupling $CoWO_4$ with gCN to form a $CoWO_4$–gCN binary nanocomposite enables the formation of a heterojunction that facilitates interfacial charge transfer, suppresses electron–hole recombination and broadens visible-light absorption, leading to enhanced photocatalytic performance. The synthesis route plays a crucial role in determining the properties of nanocomposites. Among various preparation techniques, the co-precipitation method offers significant advantages, including simplicity, low cost, scalability and precise control over composition and homogeneity [19,20]. Compared with hydrothermal, sol–gel or solid-state methods, co-precipitation allows uniform precursor mixing under mild conditions, resulting in improved interfacial contact between components and effective heterojunction formation, which are essential for photocatalytic applications [21].

In recent years, green synthesis strategies have gained importance as sustainable alternatives to conventional chemical routes [22,23]. In this work, date palm extract is employed as a natural reducing and stabilizing agent due to its abundance and richness in bioactive compounds such as polyphenols and flavonoids. These biomolecules assist in controlled nucleation, particle stabilization and surface functionalization, which can enhance light absorption and promote charge transfer, thereby improving photocatalytic activity. The environmental relevance of the synthesized nanocomposite is demonstrated through its application in dye degradation. Rose Bengal, a xanthene-based dye, is extensively used in textile dyeing, printing processes, pharmaceutical formulations, and biological staining. Significant quantities of Rose Bengal enter aquatic systems through untreated or partially treated industrial effluents, laboratory waste disposal and textile rinsing processes.

Due to its high photo-stability and complex aromatic structure, Rose Bengal persists in water bodies where it can inhibit photosynthesis, reduce dissolved oxygen levels and exert toxic effects on aquatic organisms, posing long-term ecological and health risks [24-26]. In this study, we report the green co-precipitation synthesis of a $CoWO_4$–gCN binary nanocomposite using date palm extract, followed by microwave treatment and calcination. The structural, optical and morphological properties are investigated using XRD, UV–DRS, FE-SEM, EDAX and XPS techniques. The photocatalytic activity is evaluated for the visible-light-driven degradation of Rose Bengal dye.

The enhanced degradation efficiency is attributed to the efficient heterojunction formed between $CoWO_4$ and gCN, which promotes rapid separation and migration of photogenerated charge carriers. This charge transfer process facilitates the generation of reactive oxygen species such as •OH and $\bullet O_2^-$ radicals, leading to effective oxidative degradation of Rose Bengal molecules under visible-light irradiation. Furthermore, the photo-catalyst exhibits excellent recyclability and structural stability over repeated degradation cycles, confirming its robustness and suitability for sustainable wastewater treatment applications.

II. MATERIALS AND METHODS

Sodium tungstate dihydrate ($Na_2WO_4 \cdot 2H_2O$), cobalt nitrate hexahydrate ($Co(NO_3)_2 \cdot 6H_2O$), urea, citric acid, sodium hydroxide (NaOH), and Rose Bengal dye (AR grade, C.I. No. 45440) were procured from CDH, India. All chemicals of analytical reagent grade (AR/ACS) were used as received without further purification. Double-distilled water was employed for the preparation of all stock solutions used in the experiments.

A. Preparation of Date Palm Extract

Fresh date palm fruits *(chhuwara)- Phoenix dactylifera L.* were collected from a local market in Rohtak, Haryana. The approximate geographical coordinates of the place being [28.8955° N and 76.6066° E] as latitude and longitude respectively. The seeds were isolated and the dried edible portion was meticulously cleaned using muslin fabric followed by grinding in a clean blender to obtain a uniform coarse powder. For extract preparation, 25 g of the grated coarse powder was immersed in 350 mL of distilled water and heated at 70–80 °C for 30 min with intermittent stirring. After cooling to room temperature, the mixture was filtered through Whatman filter paper No. 1. The obtained aqueous date palm extract was stored in clean glass bottles for subsequent experimental use.

B. Synthesis of bulk g-C_3N_4 (gCN)

Bulk graphitic carbon nitride was synthesized using analytical-grade urea and citric acid as starting materials without any additional purification. The two precursors were taken in an equal weight proportion (1:1) and homogenized thoroughly in a clean and dry beaker. The resulting mixture was tightly covered with aluminum foil and subjected to thermal treatment in a muffle furnace at 550 °C for 4 h to induce polymerization and condensation. After the heating process, the sample was allowed to cool naturally to room temperature. A yellow, lightweight and flaky bulk gCN material was obtained, which was subsequently ground into a fine powder and kept in desiccator for further characterization and experimental studies.

C. Synthesis of $CoWO_4$ and gCN/$CoWO_4$ NCs

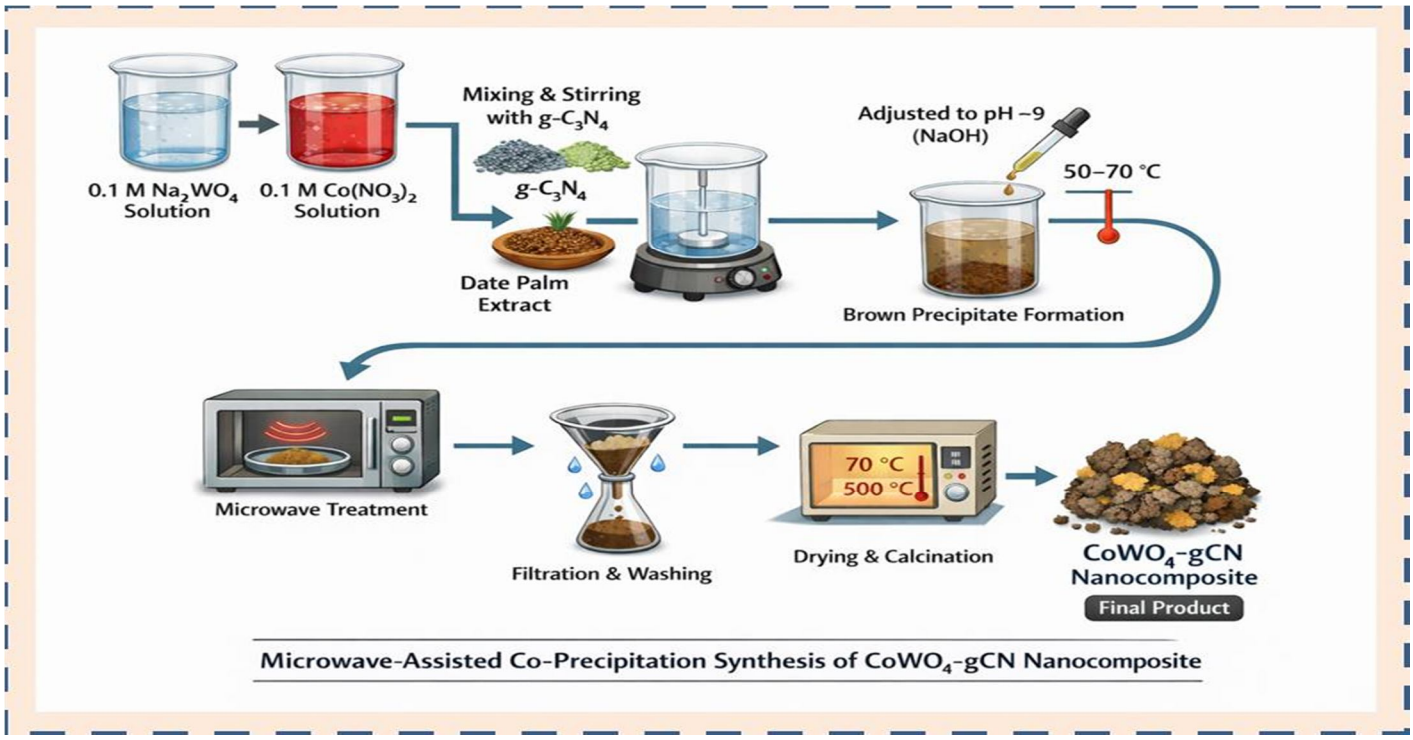

Fig. 1. Representative illustration of the microwave-assisted co-precipitation route used for the synthesis of $CoWO_4$–g-C_3N_4 binary nanocomposites, highlighting precursor mixing, bio-assisted pH control, microwave treatment and thermal calcination

The $CoWO_4$–gCN binary nanocomposite was synthesized by a co-precipitation method employing green extract (Schematic diagram as shown in Fig. 1). A 0.1 M sodium tungstate solution was prepared by dissolving 1.649 g of sodium tungstate in 30 mL of double-distilled water. Separately, a 0.1 M cobalt nitrate solution was obtained by dissolving 0.874 g of cobalt nitrate in 30 mL of distilled water, producing a bright red solution. The cobalt nitrate solution was added dropwise to the sodium tungstate solution under continuous magnetic stirring, followed by the addition of gCN (0.25, 0.50, and 0.75 g). Subsequently, 10 mL of aqueous date palm extract was introduced and the pH of the reaction mixture was adjusted to ~9 by dropwise addition of NaOH. The suspension was magnetically stirred while the temperature was gradually increased from 50 to 70 °C. The formation of brownish precipitates indicated the successful synthesis of the $CoWO_4$–gCN binary nanocomposite. The obtained product was microwave treated (a domestic microwave oven (Sharp R-219 T (W)), operating at a power of 800 W and a frequency of 2450 MHz) for 5 minutes with interval of 30 seconds which was cooled down at room temperature and later filtered and washed twice with distilled water and ethanol (75:25). Finally, the product was dried at 70 °C for 24 hr in a hot air oven and afterwards calcined at 500 °C for 120 min in muffle furnace. Lastly, the dark brown product so obtained was cooled, finely grounded and kept for characterization accordingly.

III. CHARACTERIZATION

The crystallinity and phase purity of the nanocomposites were analyzed using an X-ray diffractometer (XRD; PANalytical X'Pert Pro) equipped with Cu Kα radiation (λ = 1.54056 Å), operated at a scanning speed of 2° per minute in the 2θ range of 20°–70°. The surface morphology and elemental composition of the samples were examined using a high-resolution field-emission scanning electron microscope coupled with energy-dispersive spectroscopy (FE-SEM/EDS, Model 7610F Plus) from JEOL, where EDS spectra were recorded after proper calibration to confirm the presence and distribution of constituent elements. UV–visible diffuse reflectance and absorption measurements were performed using a PerkinElmer Lambda 1050 UV–Vis–NIR spectrophotometer to evaluate the optical response of the $CoWO_4$/gCN nanocomposites over the wavelength range of 200–850 nm. X-ray photoelectron spectroscopy (XPS) analysis was carried out using an ultra-high vacuum AXIS Supra spectrometer from Kratos Analytical Ltd, equipped with a monochromatic Al Kα X-ray source (1486.6 eV). All measurements were performed under ultra-high vacuum conditions, and Ar^+ ion sputtering was employed for surface etching and depth profiling to ensure reliable surface and near-surface

compositional analysis. For photocatalytic evaluation, the degradation of Rose Bengal dye was monitored on Lasany International UV-Vis spectrophotometer 295 with the characteristic absorption maximum (λmax) observed around 547 nm, and the systematic decrease in absorbance intensity was used for further analysis of degradation behavior and photocatalytic effectiveness.

A. Photocatalytic degradation of Rose Bengal (RB)

The photocatalytic performance of the synthesized $CoWO_4$/gCN nanocomposite was investigated using Rose Bengal (RB) dye as a model organic pollutant under visible-light irradiation. In a typical experiment, 100 mL of aqueous RB solution with an initial concentration of 20 ppm was taken in a 400 mL beaker and 0.0125 g of the photocatalyst was dispersed under continuous magnetic stirring. Prior to light exposure, the suspension was stirred in the dark for 30 min to attain adsorption–desorption equilibrium. The reaction mixture was then irradiated using two white LED flood lights (50 W each), and the photocatalytic degradation process was monitored for a total duration of 75 mins. At regular time intervals of 15 min, aliquots were withdrawn, centrifuged, and filtered to remove catalyst particles and analyzed using a Systronics 2202 UV–visible spectrophotometer. The residual concentration of RB was determined by measuring the absorbance at its characteristic maximum wavelength (~547 nm) within the 400–600 nm spectral range. The degradation efficiency was evaluated from the temporal decrease in absorbance and corresponding concentration ratios (C/C_0), confirming the effective photocatalytic degradation of Rose Bengal over the $CoWO_4$/gCN (0.05gm) nanocomposite under visible-light irradiation.

Degradation (%) was computed from the following equation:

$$\textbf{Degradation (\%)} = [(C_0 - C_t) / C_0] \times 100 \qquad (1)$$

where C_0 and C_t are the concentrations of Rose Bengal dye before and after visible light illumination.

IV. RESULTS AND DISCUSSION

A. Structural and Phase Analysis of $CoWO_4$/g-C_3N_4 (XRD)

The crystalline structure, phase purity, and structural compatibility of gCN, $CoWO_4$, and the $CoWO_4$/gCN nanocomposite were systematically examined using powder X-ray diffraction, as shown in Fig. 3.1. The XRD pattern of gCN confirms the successful formation of the layered graphitic framework, characterized by its typical diffraction features and partially amorphous nature. The XRD pattern of the as-synthesized $CoWO_4$ nanoparticles exhibits sharp and intense diffraction peaks, indicating high crystallinity and phase purity. The diffraction peaks observed at 2θ values of 15.57°, 18.99°, 23.82°, 24.66°, 30.65°, 31.46°, 36.34°, 38.55°, 41.33°, 44.35°, 45.81°, 48.75°, 50.56°, 52.06°, 54.02°, 61.76°, 63.81°, 65.08°, 68.67°, and 71.82° are indexed to the (010), (001), (–110), (011), (–111), (020), (200), (002), (200), (002), (–201), (–211), (–112), (–220), (022), (031), (–122), (–311), (222), (–231), (–140), and (–123) crystallographic planes of monoclinic wolframite-type $CoWO_4$, respectively. These reflections show excellent agreement with the standard XRD pattern of $CoWO_4$ (JCPDS Card No. 15-0867), confirming the successful formation of crystalline cobalt tungstate as in Fig. 4.1.

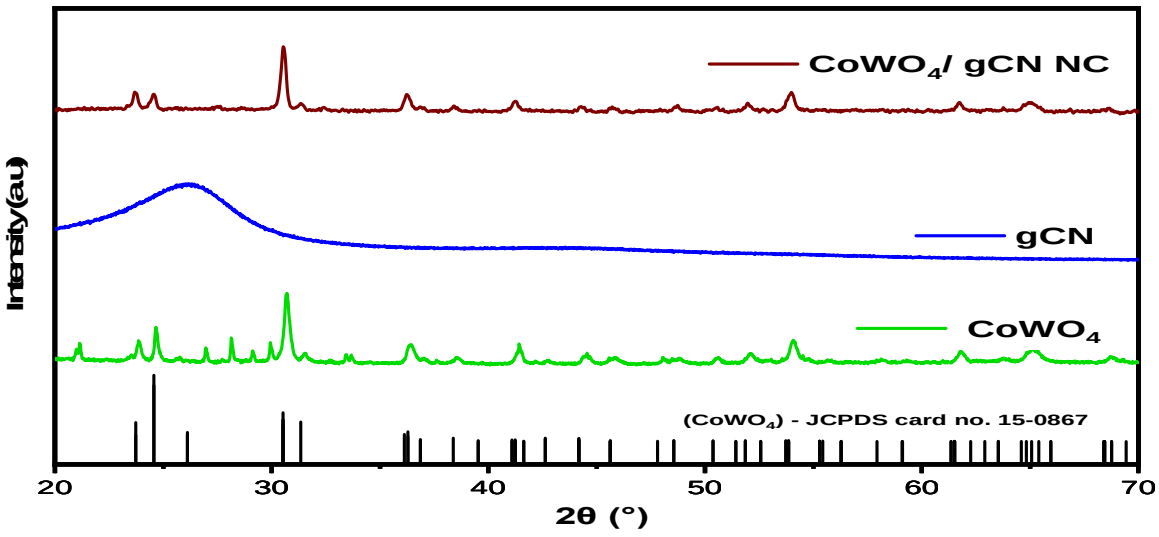

Fig. 4.1 XRD patterns of standard $CoWO_4$ (JCPDS 15-0867), $CoWO_4$, gCN and $CoWO_4$/gCN nanocomposite

In the $CoWO_4$/gCN nanocomposite, the characteristic diffraction peaks of both $CoWO_4$ and gCN are clearly retained, demonstrating the effective integration of the two components without structural distortion. The preservation of $CoWO_4$ peak positions, along with the absence of impurity-related reflections, further confirms the phase purity and strong structural compatibility of the $CoWO_4$/gCN nanocomposite.

The average crystallite size (D) of $CoWO_4$ was estimated using the Debye–Scherrer equation, given below:

$$D = 0.94\,\lambda / \beta_{1/2} \cos\theta \qquad (2)$$

where $\lambda = 1.54056$ Å is the wavelength of the incident X-ray radiation, $\beta_{1/2}$ represents the full width at half maximum (FWHM) of the diffraction peak, and θ is the corresponding Bragg angle. Using above equation, the crystallite size was calculated to be 25.12 nm.

B. Surface Chemical States and Oxidation States (XPS)

X-ray photoelectron spectroscopy (XPS) was employed to investigate the surface elemental composition and chemical states of the $CoWO_4$/gCN nanocomposite. The wide-scan survey spectrum confirms the coexistence of C, N, Co, W, and O validating the successful formation of the $CoWO_4$/gCN heterojunction as shown in the Fig. 4.2.

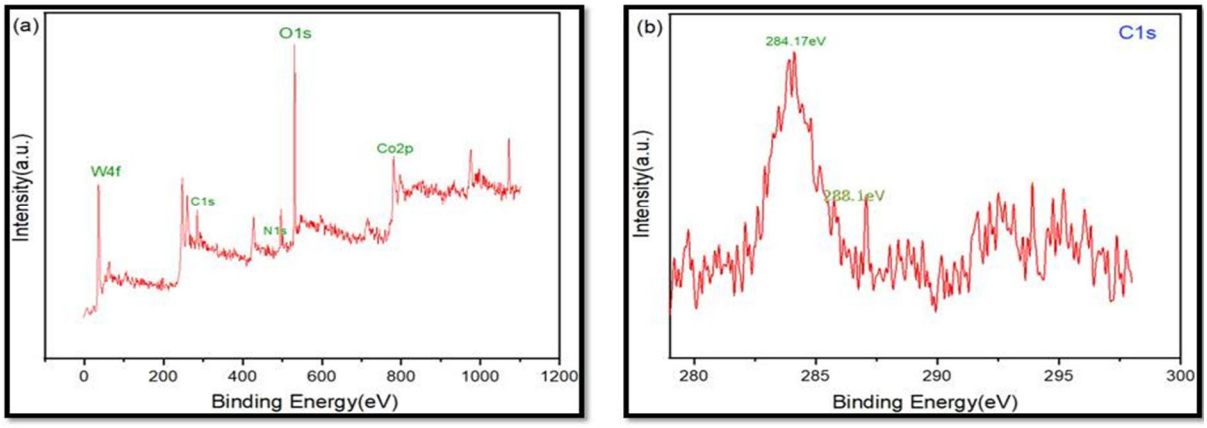

The high-resolution C 1s spectrum exhibits two characteristic peaks at 284.17 eV and 288.1 eV, corresponding to sp^2-hybridized C–C/C=C bonds and N–C=N species associated with the gCN framework. The N 1s spectrum shows a dominant peak at 399.23 eV, attributed to sp^2-hybridized aromatic nitrogen in heptazine units, indicating preservation of the gCN structure after composite formation.

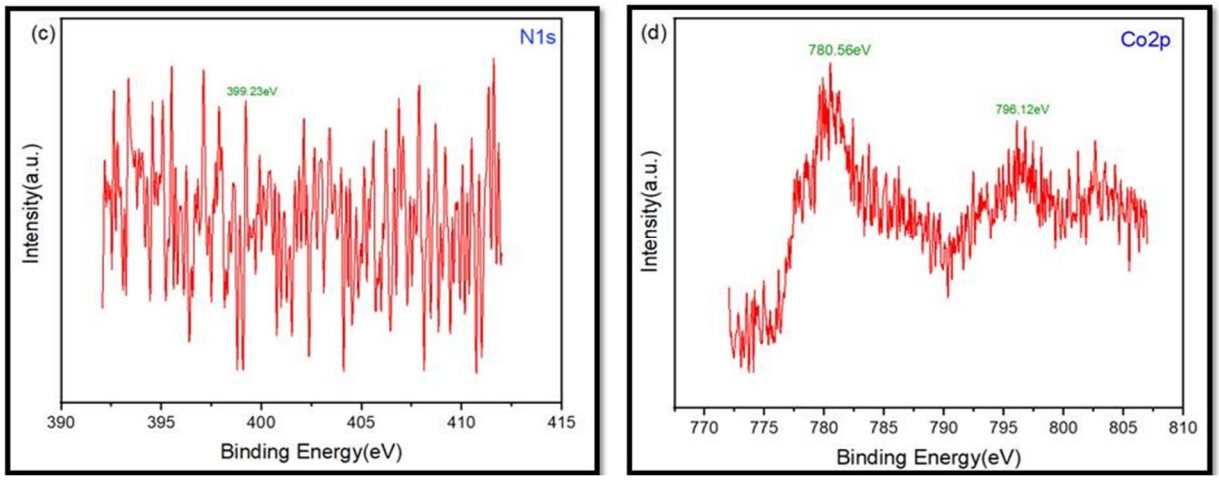

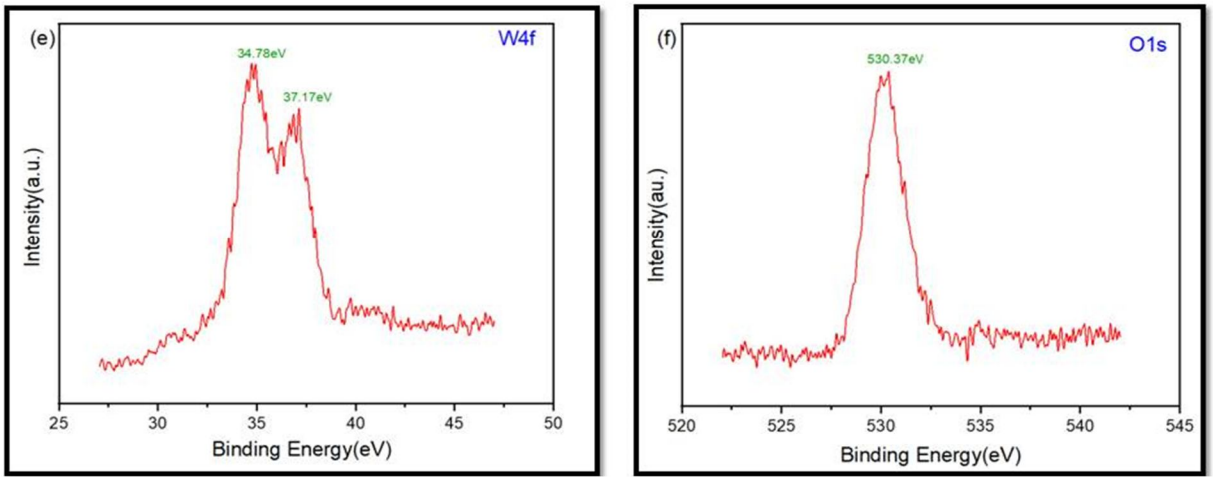

Figure 4.2 *XPS analysis of the $CoWO_4$/gCN nanocomposite: (a) survey spectrum and high-resolution spectra of (b) C 1s (c) N 1s (d) Co 2p (e) W 4f and (f) O 1s*

The Co 2p spectrum displays well-defined Co $2p_{3/2}$ and Co $2p_{1/2}$ peaks centered at ~780.56 eV and ~796.12 eV, confirming the presence of Co^{2+} species. Additionally, the W 4f spectrum reveals peaks at ~34.78 eV and ~37.17 eV, characteristic of W^{6+} oxidation states. The O 1s peak observed at ~530.37 eV is assigned to lattice oxygen and surface hydroxyl groups. These results collectively indicate strong interfacial coupling and favorable charge transfer characteristics within the $CoWO_4$/gCN nanocomposite.

C. Morphological Features and Heterojunction Formation (SEM Analysis)

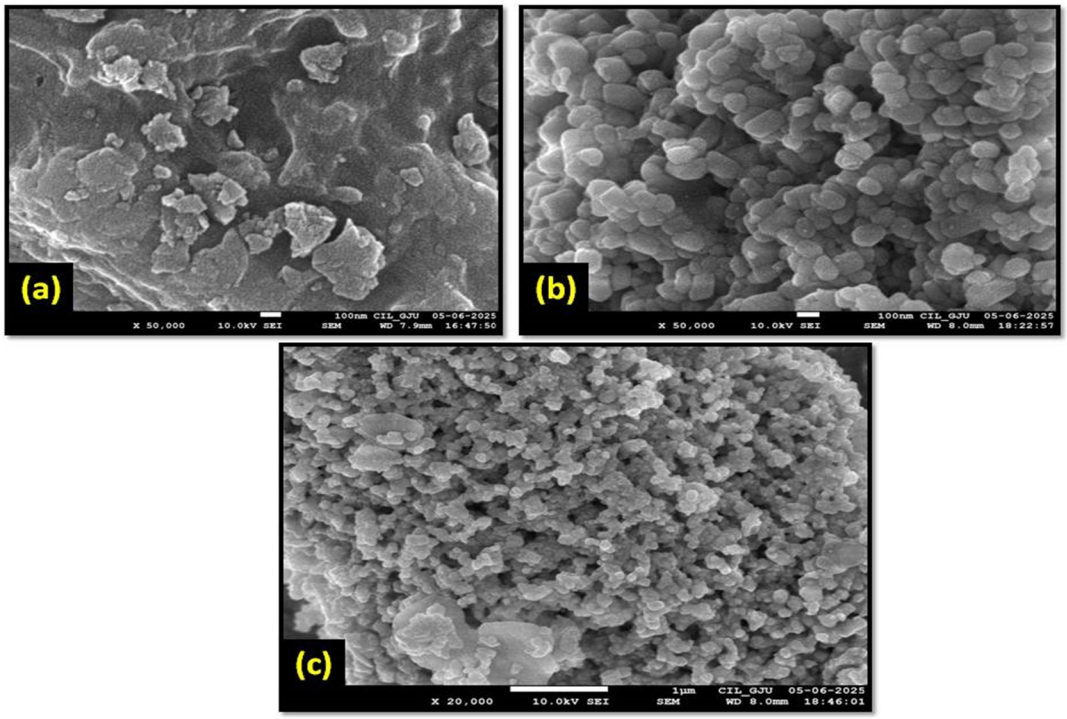

Fig. 4.3 (a), (b), (c) shows gCN, $CoWO_4$, and $CoWO_4$/gCN FE-SEM micrographs respectively.

Field-emission scanning electron microscopy (FE-SEM) was employed to examine the surface morphology of gCN, pristine $CoWO_4$ and the $CoWO_4$/gCN binary nanocomposite.

As shown in Fig. 4.3(a), the synthesized gCN exhibits a characteristic layered and sheet-like morphology composed of loosely stacked, wrinkled nanosheets, providing a large surface area with abundant anchoring sites. The FE-SEM image of pristine $CoWO_4$ Fig. 4.3(b) reveals densely packed, quasi-spherical nanoparticles with slight agglomeration, indicative of uniform nucleation during synthesis. In contrast, the FE-SEM micrograph of the $CoWO_4$/gCN nanocomposite Fig. 4.3(c) clearly demonstrates that $CoWO_4$ nanoparticles are homogeneously distributed and firmly anchored onto the gCN nanosheets. This intimate interfacial contact confirms that gCN acts as an effective supporting matrix, suppressing nanoparticle agglomeration and verifying the successful formation of a well-integrated nanocomposite architecture, which is beneficial for enhanced interfacial charge transfer [28].

D. Elemental Confirmation and Purity (EDX)

Energy-dispersive X-ray (EDX) analysis, coupled with eZAF correction, confirms the elemental composition of the synthesized materials. The pristine gCN sample exhibits only C and N signals, whereas the $CoWO_4$/gCN nanocomposite shows distinct peaks corresponding to C, N, O, Co, and W without any detectable impurity phases. The near-stoichiometric Co:W atomic ratio, together with low quantification errors (<5 % for Co and W), verifies the successful formation of the cobalt tungstate phase and its effective integration within the gCN matrix, demonstrating the high purity and compositional integrity of the nanocomposite as Fig. 4.4 (a–b).

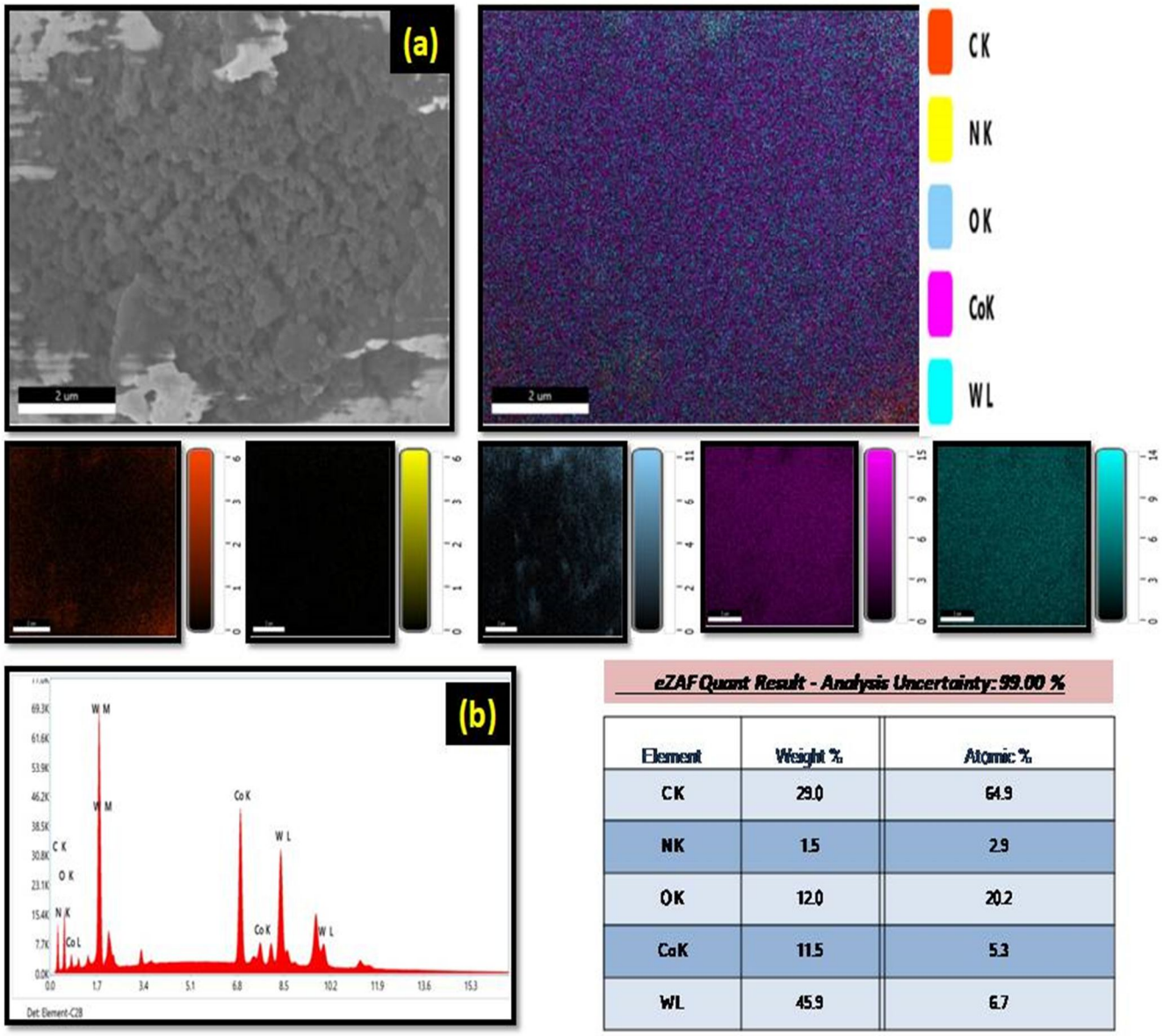

eZAF Quant Result - Analysis Uncertainty: 99.00 %

Element	Weight %	Atomic %
CK	29.0	64.9
NK	1.5	2.9
OK	12.0	20.2
CoK	11.5	5.3
WL	45.9	6.7

Fig.4.4 (a–b) EDS and eZAF-corrected elemental analysis of the $CoWO_4$/gCN nanocomposite

E. Optical Properties and Band Gap Modulation (UV–vis DRS)

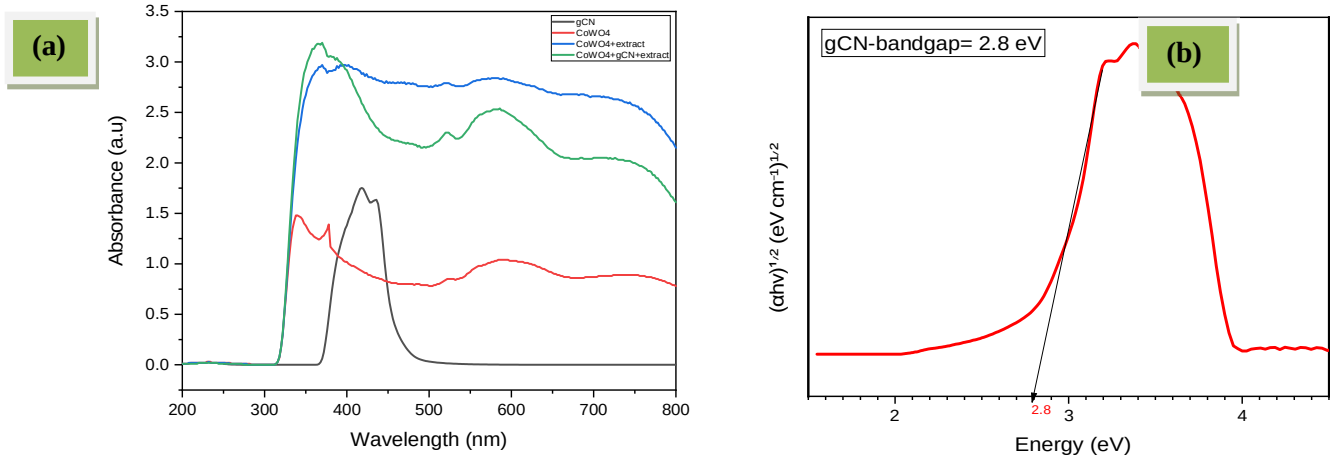

Fig. 4.5 (a) presents UV–DRS spectra of gCN, $CoWO_4$, extract-assisted $CoWO_4$, and $CoWO_4$/gCN nanocomposite, while Fig. 4.5 (b) shows the bandgap of gCN by Tauc plot

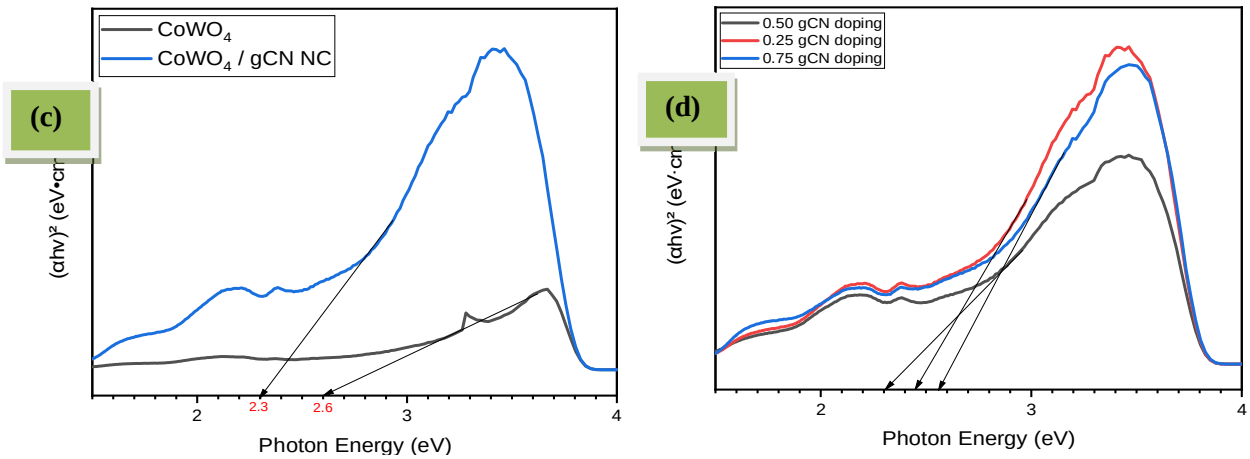

Fig. 4.5(c) – 4.5(d) show band-gap narrowing in $CoWO_4$/gCN relative to $CoWO_4$ and the effect of gCN doping level.

The photoresponse of the as-synthesized samples was investigated using UV–visible diffuse reflectance spectroscopy. As illustrated in Fig. 4.5(a), pristine $CoWO_4$, bare gCN, extract assisted $CoWO_4$ and the $CoWO_4$/gCN nanocomposite exhibit strong visible-light absorption. Bare gCN shows an absorption edge at ~450 nm, whereas the extract assisted $CoWO_4$ and $CoWO_4$/gCN nanocomposite extends up to ~750 nm, indicating a pronounced red shift and enhanced absorption intensity. The effect of gCN loading on band gap energy is shown in Fig. 4.5(d), where optimal loading (0.050 g) results in band gap narrowing, while higher loading causes agglomeration-induced widening. Band gap energies estimated using Tauc's relation Fig. 4.5(b) and 4.5(c) were 2.8 eV for gCN, 2.6 eV for pristine $CoWO_4$, 2.3 eV for as synthesized $CoWO_4$/gCN [27].

V. PHOTOCATALYTIC PERFORMANCE TOWARD ROSE BENGAL DEGRADATION

A. Time-Dependent Photodegradation of Rose Bengal

The photocatalytic activity of the as-prepared $CoWO_4$/gCN nanocomposite towards Rose Bengal (RB) degradation was evaluated under visible -light irradiation by tracking UV–visible spectral changes. A 20 ppm RB solution was used as the model pollutant and the degradation progress was monitored at its characteristic absorption maximum (λmax = 547 nm).

ISSN: 2321-9653; IC Value: 45.98; SJ Impact Factor: 7.538
Volume 14 Issue II Feb 2026- Available at www.ijraset.com

Table 5.1 Photocatalytic degradation kinetics of Rose Bengal by $CoWO_4$–gCN nanocomposite

Time (min)	Absorbance (A_t)	$C/C_0 = A_t/A_0$	Degradation (%)	$\ln(C_0/C_t) = \ln(A_0/A_t)$
0	0.89	1.000	0.00	0.000
15	0.80	0.899	10.11	0.107
30	0.74	0.831	16.85	0.185
45	0.64	0.719	28.09	0.330
60	0.15	0.169	80.15	1.781
75	0.08	0.090	81.01	2.409

Prior to illumination, 0.0125 g of the photocatalyst (synthesized binary nanocomposite) was dispersed in the dye solution and stirred in the dark for 30 min to establish adsorption–desorption equilibrium, while maintaining the solution pH in the near-neutral range (pH~7). Upon irradiation using two white LED flood lights (50 W each), the absorption intensity of RB decreased continuously with exposure time, confirming progressive dye decomposition and ~**81.01**% degradation was achieved within 75 min as shown in Table 5.1, corresponding graphs in Fig.5.

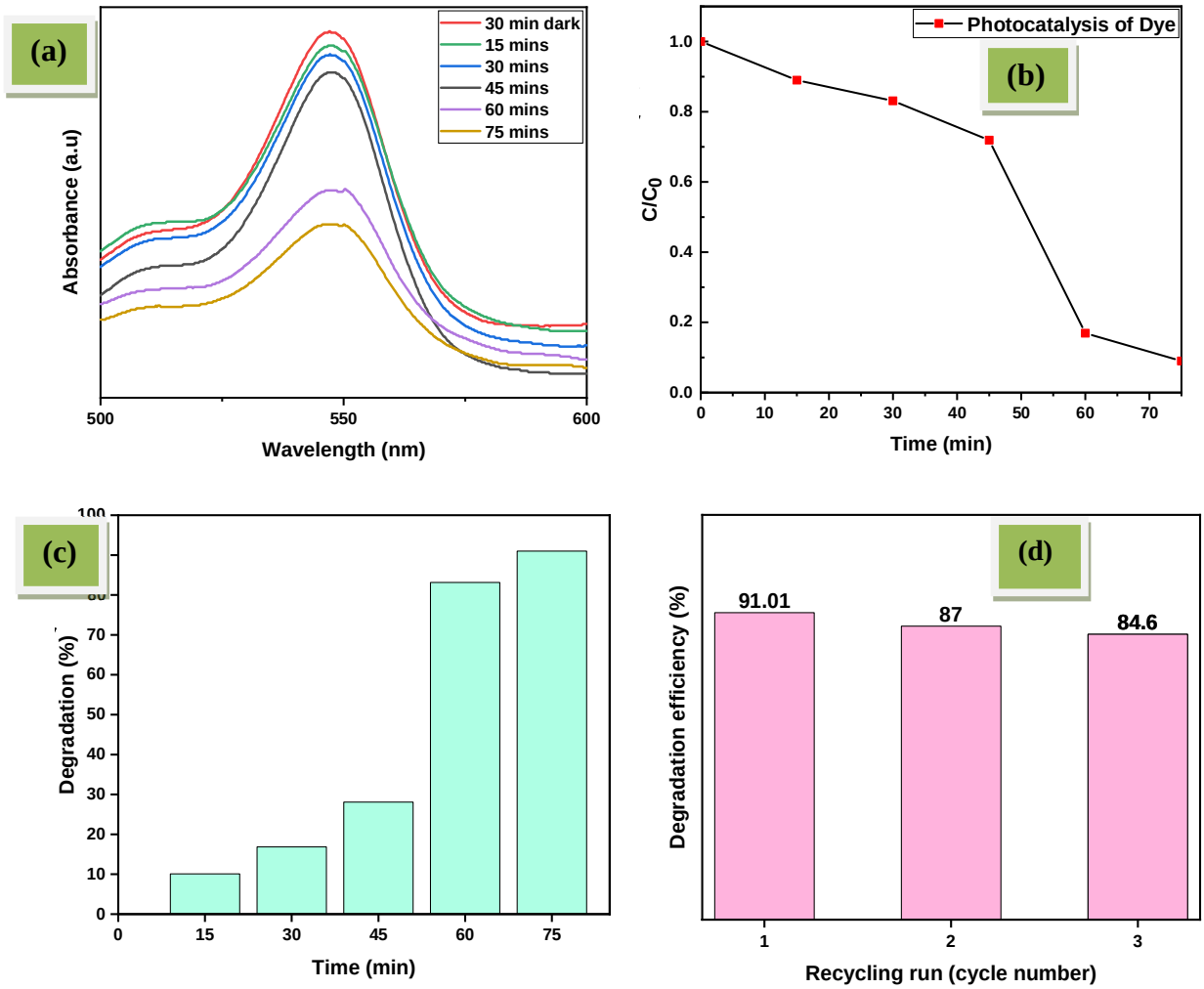

Fig. 5. Photocatalytic degradation of Rose Bengal over the $CoWO_4$/gCN nanocomposite under visible-light irradiation: (a) UV–Vis absorption spectral change (b) normalized concentration decay (C/C_0) versus irradiation time (c) degradation efficiency after 75 min (d) recyclability performance over successive cycles

The degradation kinetics were evaluated using the Langmuir–Hinshelwood pseudo-first-order model. The $\ln(C_0/Ct)$ versus time plot exhibited an overall increasing trend with slight deviation from ideal linearity ($R^2 = 0.803$), likely due to the multi-stage degradation behavior during prolonged irradiation. The apparent rate constant was estimated as $k_{app}=3.28\times10^{-2}$ min^{-1}. [29, 30].

B. Comparative Photocatalytic Study of Rose Bengal: Performance Trends

Table 5.3 Comparative photocatalytic degradation of Rose Bengal dye using various nanocomposites under different irradiation conditions

S. No.	Photocatalyst / Nanocomposite	Light Source	Time (min)	RB Degradation (%)	Mechanistic / Performance Rationale
1	g-C_3N_4 (gCN)	Visible light	120	80	Baseline photocatalyst; limited activity due to rapid electron–hole recombination
2	CuO nanoparticles	Solar light	120	78.8	Moderate visible-light photocatalytic response from pristine CuO
3	Co0.7Zn0.3Fe_2O_4 nanorods	Solar light	40	58	Morphology-dependent activity with moderate degradation efficiency
4	$CoFe_2O_4/CeO_2$ (1:4) nanocomposite	Visible light	75	89	Heterojunction-assisted charge separation enhances degradation performance [16]
5	$CoWO_4$–gCN nanocomposite (Present work)	Visible light-two white LED flood lights (50 W each)	75	81.01%	Bandgap narrowing induced by extract-assisted synthesis and efficient CoWO4/gCN heterojunction-driven charge separation

C. Reusability

Reusability and stability are key factors for evaluating photocatalysts in practical applications. Accordingly, successive cycling experiments were performed for Rose Bengal degradation over the $CoWO_4$/gCN nanocomposite under identical visible-light conditions. After each run, the catalyst was recovered by centrifugation, washed with water and ethanol, dried at 60 °C overnight, and reused. As shown in Fig. 5(d) the degradation efficiency slightly decreased from **81.01** % in the first cycle to 87% in the second and 78.6% in the third cycle. This minor decline may result from surface fouling, photocorrosion or partial loss of active sites during recovery. Overall, the $CoWO_4$/gCN nanocomposite exhibits good reusability and operational stability for Rose Bengal removal.

D. Reactive Species Trapping Experiments

To further substantiate the photocatalytic mechanism of Rose Bengal degradation over the $CoWO_4$/gCN nanocomposite, reactive species trapping experiments were correlated with the optical band-gap characteristics of the individual components. The band-gap energies of gCN, pristine $CoWO_4$ and the $CoWO_4$/gCN nanocomposite were determined to be 2.8, 2.6 and 2.3 eV, respectively, indicating enhanced visible-light absorption and improved charge-carrier utilization upon heterojunction formation.

ISSN: 2321-9653; IC Value: 45.98; SJ Impact Factor: 7.538
Volume 14 Issue II Feb 2026- Available at www.ijraset.com

Radical scavenging studies using benzoquinone, isopropyl alcohol, and ethylenediaminetetraacetic acid revealed that the addition of benzoquinone caused a pronounced suppression in photocatalytic activity, confirming superoxide radicals ($\bullet O_2^-$) as the dominant reactive species. This observation supports a Z-scheme charge-transfer mechanism, wherein photogenerated electrons accumulated in the conduction band of gCN—favored by its suitable band structure—effectively reduce dissolved oxygen to $\bullet O_2^-$ radicals, while recombination with holes from $CoWO_4$ is suppressed. The moderate inhibition observed in the presence of isopropyl alcohol suggests that hydroxyl radicals (•OH), generated via hole-mediated oxidation processes at the $CoWO_4$ valence band, play a secondary role. Additionally, partial activity loss upon EDTA addition confirms the involvement of photogenerated holes in direct oxidation pathways. Collectively, the reduced band gap of the $CoWO_4$/gCN nanocomposite and the scavenger results coherently validate a Z-scheme mechanism that promotes efficient charge separation and enhanced reactive oxygen species generation, leading to superior photocatalytic degradation of Rose Bengal.

E. Dominant Reactive Species and Mechanistic Implications

Based on the radical scavenging results, the relative contribution of reactive species in the photocatalytic degradation of Rose Bengal over the $CoWO_4$/gCN nanocomposite follows the order: $\bullet O_2^- > h^+ > \bullet OH$ (as shown in Fig. 5.5) confirming superoxide-dominated Z-scheme photocatalysis over $CoWO_4$/gCN. At 75 min, the inhibition followed the order BQ (47.01%) > EDTA (25.01%) > IPA (~8%), confirming $O_2\bullet^-$ as the dominant oxidative species.

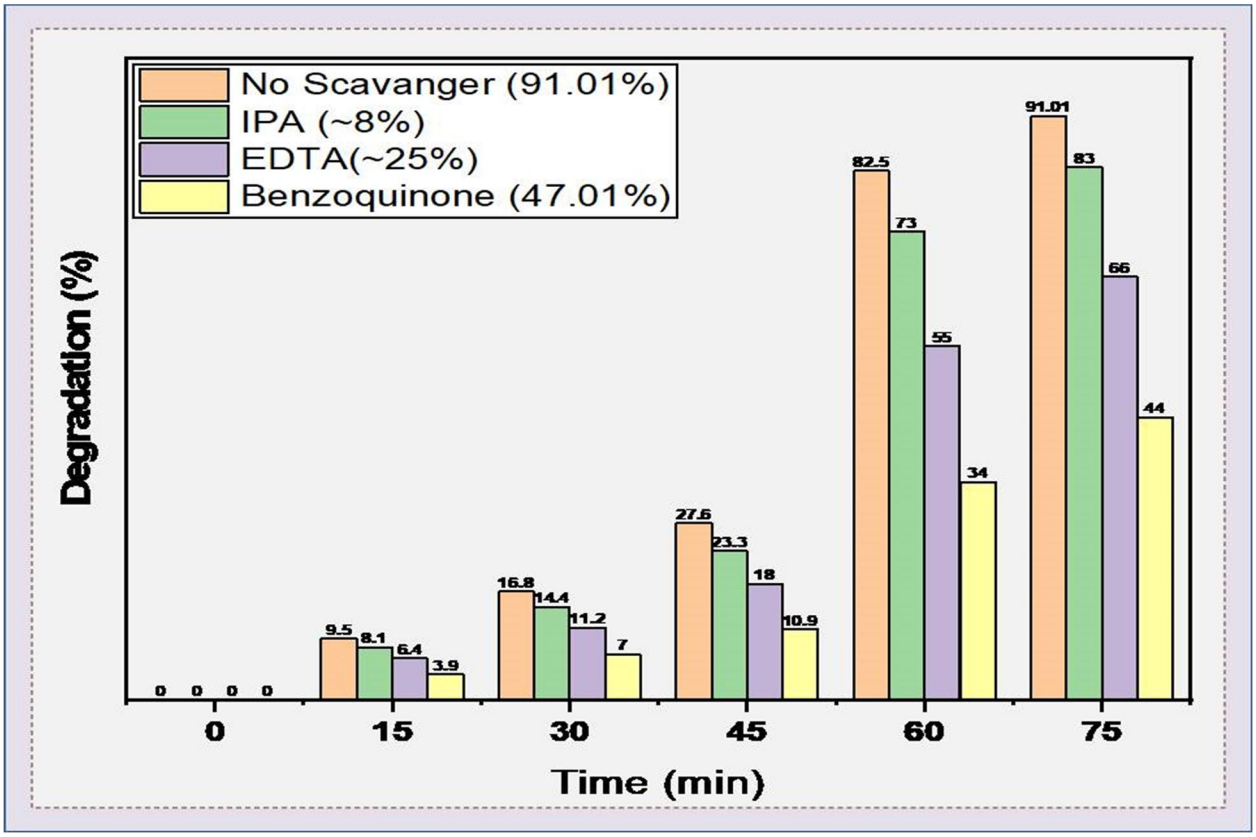

Fig. 5.5 Radical scavenger effect on Rose Bengal degradation over $CoWO_4$/Gcn

These findings clearly indicate that the photocatalytic degradation process is primarily governed by a superoxide-radical-driven pathway. The effective charge separation at the $CoWO_4$/gCN heterojunction suppresses electron–hole recombination, thereby increasing the availability of conduction-band electrons for oxygen reduction. This enhanced generation of superoxide radicals ultimately promotes efficient mineralization of Rose Bengal under visible-light irradiation.

F. Proposed Z-scheme photocatalytic mechanism for Rose Bengal degradation

On the basis of band-edge alignment and the reactive-species trapping results, a Z-scheme charge-transfer pathway is proposed for the $CoWO_4$/gCN heterojunction under visible-light irradiation.

ISSN: 2321-9653; IC Value: 45.98; SJ Impact Factor: 7.538
Volume 14 Issue II Feb 2026- Available at www.ijraset.com

Upon excitation, electrons in the CB of $CoWO_4$ preferentially recombine with holes in the VB of gCN at the interface, which suppresses non-productive recombination and preserves the strongly reducing electrons in the CB of gCN and the strongly oxidizing holes in the VB of $CoWO_4$. The retained electrons on gCN reduce dissolved O_2 to generate $\bullet O_2^-$, identified as the dominant oxidative species by the pronounced inhibition in the presence of benzoquinone. In parallel, holes accumulated on $CoWO_4$ contribute to Rose Bengal oxidation directly and/or via limited •OH formation, consistent with the partial suppression observed with EDTA and IPA. Overall, the heterojunction enhances visible-light activity by maintaining strong redox ability and promoting a $\bullet O_2^-$-driven degradation pathway.

G. Reaction Pathway for Photocatalytic Rose Bengal Degradation

Upon visible-light irradiation, the $CoWO_4$/gCN heterojunction undergoes photoexcitation, generating electron–hole pairs in both semiconducting components. Owing to the Z-scheme charge-transfer pathway, the photogenerated electrons in the conduction band of $CoWO_4$ recombine with the holes in the valence band of gCN at the interface, thereby preserving the strongly reducing electrons in the conduction band of gCN and the highly oxidizing holes in the valence band of $CoWO_4$. The key photocatalytic reactions involved in Rose Bengal degradation can be expressed as follows:

Photoexcitation:

$$\mathbf{CoWO_4/gCN + h\nu \rightarrow e^- + h^+}$$

Generation of superoxide radicals:

$$\mathbf{e^- (CB, gCN) + O_2 \rightarrow \bullet O_2^-}$$

Formation of secondary reactive species:

$$\mathbf{\bullet O_2^- + H_2O \rightarrow \bullet HO_2 + \bullet OH}$$

Hole-driven oxidation reactions:

$$\mathbf{h^+ (VB, CoWO_4) + H_2O / OH^- \rightarrow \bullet OH}$$

Degradation of Rose Bengal:

$$\bullet O_2^- / h^+ / \bullet OH + \text{Rose Bengal} \rightarrow \text{intermediates} \rightarrow \text{mineralized products } (CO_2, H_2O, \text{inorganic ions})$$

Among these species, superoxide radicals act as the primary oxidizing agents, while photogenerated holes and hydroxyl radicals contribute synergistically to the degradation process. This reaction pathway is in good agreement with the scavenger studies and the proposed Z-scheme charge-transfer mechanism as in Fig. 5.7.

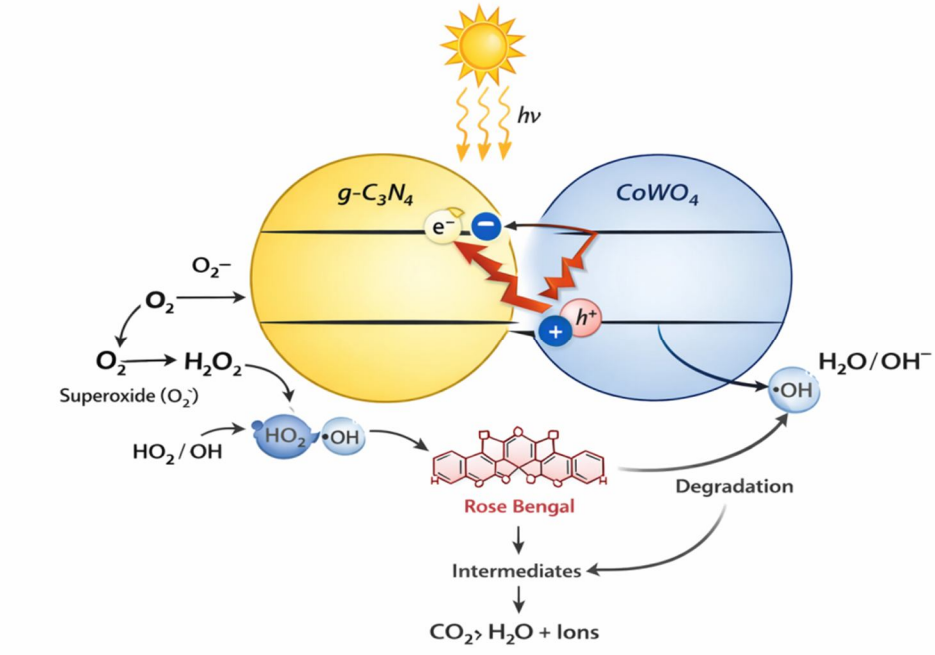

Fig. 5.7 Schematic illustration of the Z-scheme photocatalytic mechanism for RB degradation

VI. CONCLUSIONS

Overall, a visible-light-responsive $CoWO_4$/gCN nanocomposite was successfully prepared through a microwave-assisted co-precipitation route. Structural characterization confirmed the formation of monoclinic $CoWO_4$ and its intimate integration with the gCN framework. The nanocomposite exhibited enhanced optical absorption with a narrowed band gap, promoting improved charge utilization under irradiation. As a result, efficient photocatalytic degradation of Rose Bengal was achieved within a short irradiation time, following pseudo-first-order kinetics. Radical trapping experiments indicated that superoxide radicals played the dominant role in the degradation pathway. Moreover, the photocatalyst demonstrated good recyclability over multiple cycles, highlighting its stability. Collectively, the $CoWO_4$/gCN heterostructure represents a promising and reusable photocatalytic platform for sustainable wastewater remediation under visible light.

REFERENCES

[1] S. Shoran, S. Chaudhary, A. Sharma, Photocatalytic dye degradation and antibacterial activities of CeO_2/g-C_3N_4 nanomaterials for environmental applications, Environ. Sci. Pollut. Res. 30 (2023) 98682–98700.
[2] M. Jeyakanthan, U. Subramanian, R.B. Tangsali, Enhanced photoluminescence of $CoWO_4$ in $CoWO_4$/$PbWO_4$ nanocomposites, J. Mater. Sci.: Mater. Electron. 29 (2018) 1914–1924.
[3] E.D.M. Isa, N.W.C. Jusoh, A.A.M. Rodzi, Enhanced simultaneous degradation of simulated dyes using ZnO/GCN heterojunction photocatalyst, Environ. Sci. Pollut. Res. 30 (2023) 116921–116933.
[4] S. Iqbal, M. Javed, S.S. Hassan, S. Nadeem, A. Akbar, M.T. Alotaibi, R.M. Alzhrani, N.S. Awwad, H.A. Ibrahium, A. Mohyuddin, Binary Co@ZF/S@GCN S-scheme heterojunction enriching spatial charge carrier separation for efficient removal of organic pollutants under sunlight irradiation, Colloids Surf. A Physicochem. Eng. Asp. 636 (2022) 128177.
[5] M.A.S. Salem, A.M. Khan, Y.K. Manea, A novel nano-hybrid carbon architecture as a chemosensor for natural hazards: active adsorption of Rose Bengal dye and ppb-level detection of hazardous pollutants, J. Environ. Chem. Eng. 10 (2022) 107032.
[6] Sonia, Sheetal, H. Kumari, S. Sharma, S. Chahal, S. Duhan, A. Kumar, P. Kumar, Magnetic cobalt ferrite–tin oxide nanocomposites for efficient photocatalytic dye degradation, Water Air Soil Pollut. 236 (2025) 602.
[7] D.R. Paul, S.P. Nehra, Graphitic carbon nitride: a sustainable photocatalyst for organic pollutant degradation and antibacterial applications, Environ. Sci. Pollut. Res. 28 (2021) 3888–3896.
[8] N.T.M. Huong, P.T.T. Hoai, D.T.M. Hanh, T. Kim, P.T. Huong, Exploring Cu-doped graphitic carbon nitride for treatment of dye pollutants in textile wastewater: benefits and limitations, Diam. Relat. Mater. 146 (2024) 111160.
[9] O.O. Akintunde, J. Hu, M.G. Kibria, S. Pogosian, G. Achari, A facile synthesis of GCN/ZnO–Cu nanocomposite and evaluation of its performance for photocatalytic degradation of organic pollutants and wastewater disinfection under visible light, Chemosphere 344 (2023) 140287.
[10] Sonu, V. Dutta, A. Sudhaik, A.A.P. Khan, T. Ahamad, P. Raizada, S. Thakur, A.M. Asiri, P. Singh, GCN/$CuFe_2O_4$/SiO_2 photocatalyst for photo-Fenton-assisted degradation of organic dyes, Mater. Res. Bull. 164 (2023) 112238.
[11] P. Nancy Dayana, M. John Abel, P.F.H. Inbaraj, S. Sivaranjani, R. Thiruneelakandan, J. Joseph Prince, Zirconium-doped copper ferrite ($CuFe_2O_4$) nanoparticles for enhanced visible-light-responsive photocatalytic degradation of Rose Bengal and indigo carmine dyes, J. Cluster Sci. 33 (2022) 1739–1749.
[12] X.A. López, A.F. Fuentes, M.M. Zaragoza, J.A. Díaz Guillén, J. Salinas Gutiérrez, A. López Ortiz, V. Collins-Martínez, Synthesis, characterization and photocatalytic evaluation of MWO_4 (M = Ni, Co, Cu and Mn) tungstates, Int. J. Hydrogen Energy 41 (2016) 23312–23317.
[13] S. Balasurya, S. Alfarraj, L.L. Raju, A. Chinnathambi, S.A. Alharbi, A.M. Thomas, S.S. Khan, Novel $CoWO_4$–Ag_2MoO_4 nanocomposites: synthesis, enhanced photocatalytic activity under visible-light irradiation and antimicrobial performance, Surf. Interfaces 25 (2021) 101237.
[14] B. Maddah, F. Jookar-Kashi, M. Akbari, Facile precipitation synthesis of pure Fe_3O_4/$CoWO_4$ nanocomposites and investigation of their photocatalytic and antimicrobial activity, J. Mater. Sci.: Mater. Electron. 29 (2018) 13723–13730.
[15] O. Raina, R. Manimekalai, Photocatalysis of cobalt zinc ferrite nanorods under solar light, Res. Chem. Intermed. 44 (2018) 5941–5951.
[16] Sonia, A. Kumar, P. Kumar, Efficient $CoFe_2O_4$/CeO_2 nanocomposites for photocatalytic dye degradation, J. Mater. Sci.: Mater. Electron. 34 (2023) 1870.
[17] A.H. Gharbi, H. Hemmami, S.E. Laouini, A. Bouafia, I. Ben Amor, S. Zeghoud, M.T. Gherbi, A. Ben Amor, F. Alharthi, J.A.A. Abdullah, Novel CuO–SiO_2 nanocomposites: synthesis, kinetics, recyclability, high stability and photocatalytic efficiency for Rose Bengal dye removal, Transition Met. Chem. 49 (2024) 195–213.
[18] S. Roy, J. Darabdhara, M. Ahmaruzzaman, ZnO-based Cu metal–organic framework (MOF) nanocomposite for boosting and tuning photocatalytic degradation performance, Environ. Sci. Pollut. Res. 30 (2023) 95673–95691.
[19] F.A. Alharthi, H.S. Alanazi, K.M. Alotaibi, N. Ahmad, Photodegradation of methylene blue and Rose Bengal employing g-C_3N_4/$ZnWO_4$ nanocatalysts under ultraviolet light irradiation, J. Nanopart. Res. 24 (2022) 125.
[20] A. Khatri, P.S. Rana, Visible-light-assisted photocatalysis of methylene blue and Rose Bengal dyes by iron-doped NiO nanoparticles prepared via chemical co-precipitation, Physica B: Condens. Matter 579 (2020) 411905.
[21] P.P. Vhangutte, A.J. Kamble, R.A. Madhale, M.U. Patil, P.D. Bhange, V.L. Patil, A.M. Yelpale, D.S. Bhange, Solution combustion synthesis and exploration of chromium reduction and organic dye degradation using cobalt tungstate ($CoWO_4$) nanoparticles, Physica B: Condens. Matter 689 (2024) 416182.
[22] H.V.S.B. Azevêdo, R.A. Raimundo, L.S. Ferreira, M.M.S. Silva, M.A. Morales, D.A. Macedo, U.U. Gomes, D.G.L. Cavalcante, Green synthesis of $CoWO_4$ powders using agar-agar from red seaweed (Rhodophyta): structure, magnetic properties and battery-like behavior, Mater. Chem. Phys. 242 (2020) 122544.
[23] J. Komara, J.P. Karumuri, B.S.S. Naik, Green synthesis of copper oxide nanoparticles using Solanum melongena seed extract and its applications in Rose Bengal degradation, antibacterial activity, catalytic reduction, and antioxidant performance, Hybrid Adv. 7 (2024) 100304.
[24] Z.-B. Lv, J. Feng, R.-J. Zhao, J.-J. Shen, W.-W. Yang, Visible-light-driven photocatalytic degradation of ibuprofen by Cu-doped tubular C_3N_4: mechanisms, degradation pathway, and DFT calculation, Chemosphere 358 (2024) 142106.

[25] F.A. Alharthi, H.S. Alanazi, K.M. Alotaibi, N. Ahmad, Photodegradation of methylene blue and Rose Bengal employing g-C_3N_4/$ZnWO_4$ nanocatalysts under ultraviolet light irradiation, J. Nanopart. Res. 24 (2022) 125.
[26] E. Kamaraj, S. Somasundaram, K. Balasubramani, M.P. Eswaran, R. Muthuramalingam, S. Park, Facile fabrication of CuO–Pb_2O_3 nanophotocatalyst for efficient degradation of Rose Bengal dye under visible-light irradiation, Appl. Surf. Sci. 433 (2018) 206–212.
[27] S. Lakshmi Prabavathi, K. Govindan, K. Saravanakumar, A. Jang, V. Muthuraj, Construction of heterostructure $CoWO_4$/g-C_3N_4 nanocomposite as an efficient visible-light photocatalyst for norfloxacin degradation, J. Ind. Eng. Chem. 80 (2019) 558–567.
[28] P. Taneja, S. Sharma, A. Umar, S.K. Mehta, A.O. Ibhadon, S.K. Kansal, Visible-light driven photocatalytic degradation of brilliant green dye based on cobalt tungstate ($CoWO_4$) nanoparticles, Mater. Chem. Phys. 211 (2018) 335–342.
[29] A.V.K. Amritha, S. Badhulika, Fabrication and characterization of $ZnWO_4$/$CoWO_4$ heterojunction for multispectral photodetection on flexible substrates, Sens. Actuators A Phys. 374 (2024) 115463.
[30] S. Lakshmi Prabavathi, K. Govindan, K. Saravanakumar, A. Jang, V. Muthuraj, Construction of heterostructure $CoWO_4$/g-C_3N_4 nanocomposite as an efficient visible-light photocatalyst for norfloxacin degradation, J. Ind. Eng. Chem. 80 (2019) 558–567.

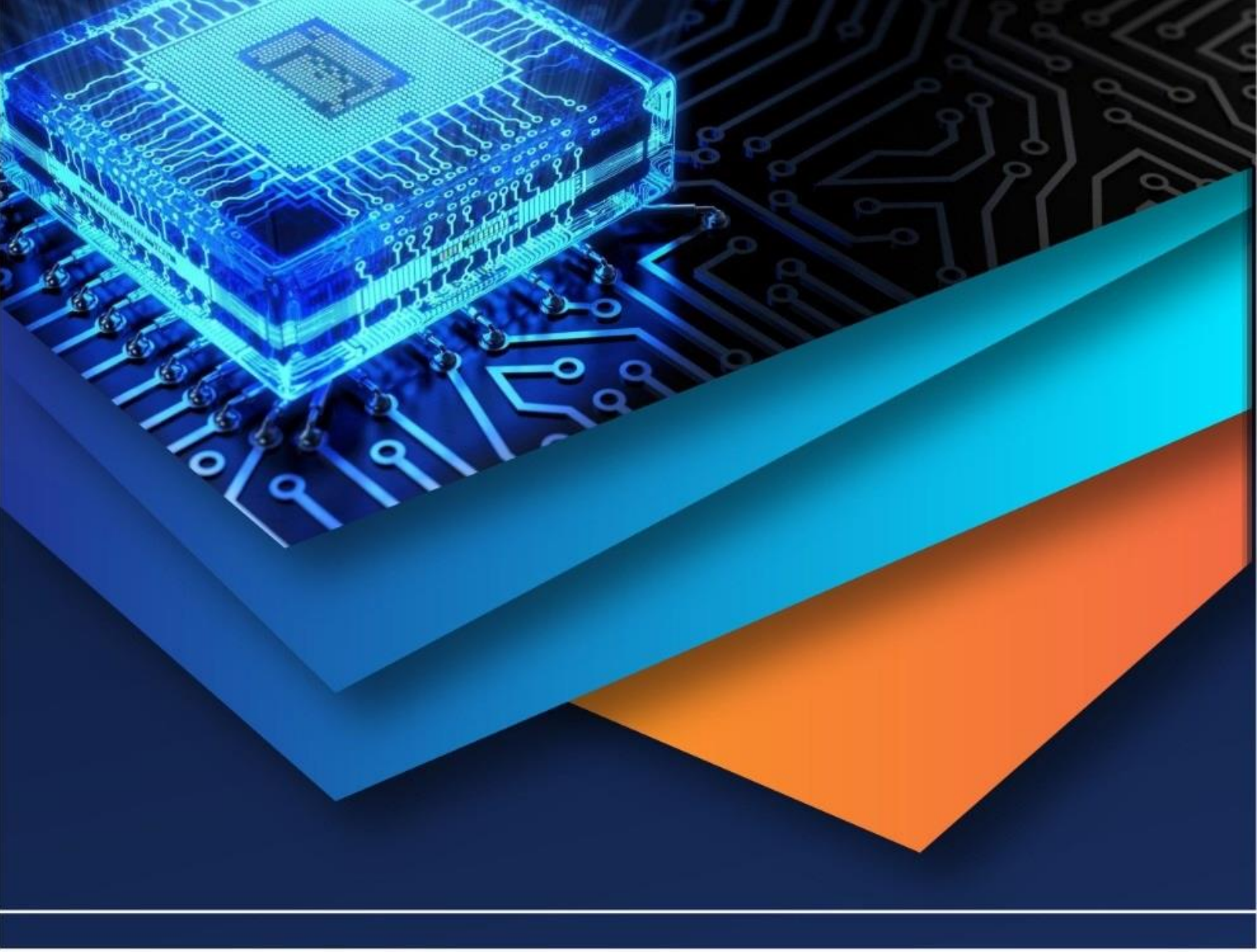

10.22214/IJRASET

45.98

IMPACT FACTOR: 7.129

IMPACT FACTOR: 7.429

INTERNATIONAL JOURNAL FOR RESEARCH

IN APPLIED SCIENCE & ENGINEERING TECHNOLOGY